International Journal of Theoretical Physics, Vol. 24, No. 6, 1985

Isomorphic Shell Model for Closed-Shell Nuclei

G. S. Anagnostatos[1]

Received March 30, 1984

The classical part of the isomorphic model for closed-shell nuclei is presented based on two physical assumptions, namely (a) the nucleons of a closed shell nucleus, considered at their most probable positions, are in an instantaneous dynamic equilibrium on spherical shells, and (b) the dimensions of the shells are determined by their close packing given that a neutron and a proton are represented by hard spheres of definite sizes. The first assumption leads to the instantaneous angular structure, and the second to the instantaneous radial structure of closed-shell nuclei. Applications of the model coming from this classical part alone and presented here are structural justification of all magic numbers, neutron (proton) and charge rms radii, nuclear densities of closed-shell nuclei, and Coulomb, kinetic, and binding energies. All the predictions are in good agreement with experimental data. A characteristic novelty of the isomphic model is that assumption (a) is related to the independent particle model, and assumption (b) to the liquid-drop model. The isomorphic model may provide a link between these two basic nuclear physics models since it incorporates features of both.

1. INTRODUCTION

Even though there is not yet an exact theory of nuclear structure, there are some generally accepted concepts that have engendered the development of a number of successful models. Among these models, the isomorphic model (IM) has a unique feature, its extensive use of symmetry, a concept that has proved to be highly successful in many other areas of physics and chemistry. Specifically, the IM is a microscopic nuclear structure model for the ground state, and it has been developed independently of the established shell model and the collective models. In fact, in the IM we are concerned mainly with the closed-shell nuclei which constitute the core of all nuclei.

[1]Tandem Accelerator Laboratory, Nuclear Research Center "Demokritos," Athens, Greece.

0020-7748/85/0600-0579$04.50/0

Thus, the IM deals with the depth of the Fermi sea,[2,3] which is not the subject matter of either the independent particle models or the collective models. Therefore the IM should *not* be considered as a competitor to any of the above models but rather as a common complementary part of them.

While the IM is known through several publications (Anagnostatos, 1973; 1977; 1978; 1980a, b; de Boer and Mang, 1973; Anagnostatos et al., 1980; 1981; Anagnostatos and Panos, 1982), the present study attempts to put it on a firmer footing than before by intoducing into it a new fundamental physical assumption, the close packing of nuclear shells. This assumption has strengthened the physical basis of the IM substantially and has thus led to a high accuracy of its predictions. To put it otherwise, the aforementioned new hypothesis underlines a simple structural rule which reproduces the size and other properties of nuclei all the way up to Pb and at the same time implies a common origin of both the independent particle and the collective models. Consequently this work may provide a picture of the nucleus which can unite the available information about nuclei into a consistent body of knowledge.

The IM is divided into three basic parts: the classical, the semiclassical, and the quantum mechanical parts. The present paper has as its subject the classical (geometrical) part which, due to the introduction of the close packing assumption, is presented and applied here in a way that is more satisfactory from a physical point of view than the one adopted in our previous works. Indeed, when one examines the most probable positions of all particles of a particular shell, a real form results, a specific high-symmetry polyhedron of definite size. Now, as will be shown in this contribution, the incorporation into our model of the assumption of the close packing of nuclear shells reveals that the different concentric polyhedral shells of a closed-shell nucleus have definite highly symmetric relationships to each other, thus permitting one to form a mental image of the structure of each of the closed-shell nuclei. We have found that the properties of such an imaginary structure for any closed-shell nucleus reproduce with high accuracy the experimentally known properties for that nucleus itself.

Although in this contribution we focus on the classical part of the IM, we wish to say a few words about the other two parts of our model. The semiclassical part of the IM deals with an isomorphism (one-to-one correspondence) which can be established between the sets of quantum numbers

[2]There are some other models that deal with the structural picture of the nucleus, but are essentially different from the isomorphic model. See, e.g., Cook (1976), Robson (1978), Margenau (1941), and Pauling (1965a).

[3]What we really know about the nucleus refers mostly to the valence nucleons on top of the Fermi sea and we know very little of what is really happening in the depths of the fermi sea (Wilkinson, 1977).

(n, l, m, s, τ) and the points of the point space made up of the vertices of the polyhedra employed to represent the average shapes of nuclear shells. The name of the model is taken from this isomorphism. The quantum mechanical part introduces a new potential and solves the Schrödinger equation for that potential. No adjustable parameters are utilized; instead the boundary conditions and the constants involved in the wave function, derived from the Schrödinger equation for a particular nucleon, are determined from the coordinates of the point (vertex) having, according to the isomorphism made, the same set of quantum numbers as that nucleon.

Our remark that high symmetry and ground-state nuclear structure might be correlated is supported by Moszkowski's (1957) statement that quantum states of lowest energy exhibit simple shapes which are determined by the inherent symmetry of the system, and that nuclear interactions (short-ranged, attractive) favor states of maximum spatial symmetry. We are also aware that this polyhedral specification of symmetry, at first sight, lends itself to a classical treatment only. At the same time we know that any realistic representation of nuclear structure must follow quantum mechanics. As Inglis (1969) has remarked, however, the development of a nuclear model may follow a pictorial approach in the spirit of the correspondence principle that there is at least a rough correspondence between quantum mechanics and quantized classical physics (e.g., classical quantization of space implied by polyhedral shell structure, as used in our model) that gets better as quantum numbers get larger. Thus, a geometrical understanding of nuclear stucture has a rational basis. At this stage we wish to point out that current nuclear quantum mechanical models may be interpretable in crystallographic terms and that such understanding could show that nuclear shell structure is more general than the independent-particle basis upon which it currently rests.

Our paper is organized as follows. In Section 2 we describe the assumptions and development of the new IM, which is the main purpose of our work. Section 3 gives an account of some of the main applications of the model to the following nuclear properties: nuclear shells and magic numbers, nuclear radii, nuclear density, and kinetic, Coulomb, and binding energies. Section 4 offers a comparison between the predictions of the model and those of other nuclear structure models. Section 5 consists of the summary and conclusions. There are also five appendices.

2. DEVELOPMENT OF THE IM

In this section the IM is developed following a deductive process based on two assumptions. As a result, it is found that the different shells of a closed-shell nucleus have instantaneous dynamic shapes represented by

specific concentric high symmetry polyhedra of definite sizes, derived from one another (see Figure 1). The vertices of these polyhedral shells, representing most probable nucleon positions, form a maximum spatial symmetry point-space.

2.1. Assumptions

The IM is based on two assumptions:

(a) The neutrons (protons) of a closed neutron (proton) shell at the ground state, considered at their *most probable positions*, are in *dynamic equilibrium* on a sphere.

(b) The dimensions of the shells of a closed-shell nucleus at the ground state are determined by the *close-packing of the shells* themselves, provided that a neutron and a proton are represented by *hard spheres* of definite sizes (i.e., $r_n = 0.974$ fm and $r_p = 0.860$ fm, which constitute the only parameters of the model).

Assumptions (a) and (b) are independent of each other and appear to be plausible and both consistent with the least energy principle. The concept that the nucleus has a shell structure is inherent in assumption (a), and, as we shall see shortly, assumption (a) alone leads to the angular part of the instantaneous nuclear structure of the closed-shell nuclei from ^{4}He to ^{208}Pb, while from assumption (b) the radial part of this structure is derived. In the following, the above two assumptions are discussed with the aim of clarifying their physical basis.

The main assumption of the simple shell model (usually very successful in spherical nuclei), viz., that the individual nucleons in a nucleus more relatively freely in well-defined single-particle orbitals, may be here understood in terms of a dynamical equilibrium in the following sense. Each nucleon in a nucleus at the ground state is in a dynamic equilibrium with the other nucleons, and, as a consequence, its motion may be described independently of the motion of the other nucleons.

In particular, the model assumes a specific equilibrium of nucleons, which is valid whatever the law of nuclear force may be. Clearly our assumption does not preclude the existence of an equilibrium of nucleons that corresponds strictly to the exact law of the nuclear force. In fact, if we denote by S the set of equilibria in the sense of our hypothesis and by S_1 the set of equilibria pertaining to the particular law of the nuclear interaction, then

$$S \subseteq S_1 \tag{1}$$

Evidently, equation (1) could lead to some contradictions with experimental data about nuclear shells and other properties since we might overlook some cases of equilibrium. However, assumption (a) seems rather justified,

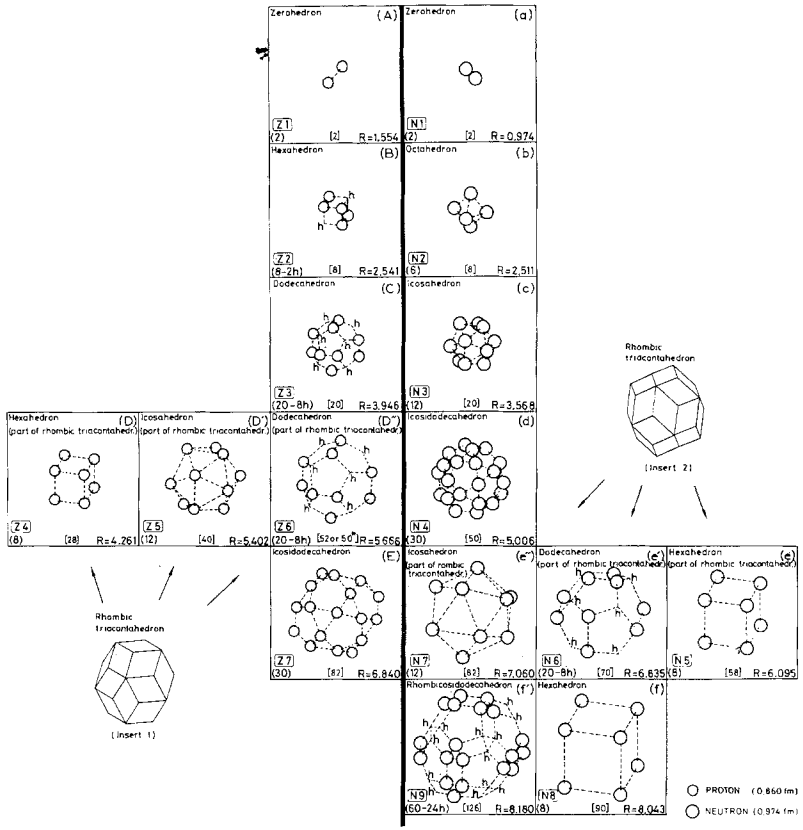

Fig. 1. Instantaneous dynamic average forms of nuclear shells from ^{4}He to ^{208}Pb presented by equilibrium polyhedra. Polyhedra lying on the left of the heavy central vertical line stand for proton shells, while those on the right stand for neutron shells, with a correspondence between them such that next to a proton (neutron) polyhedron (in each of the levels of the figure, which are labelled A-F for protons and a-f for neutrons) a neutron (proton) polyhedron exists that has the same rotational group (i.e., it is its reciprocal in geometrical language). The angular vertex distribution of the rhombic triacontahedron in insert 1 is identical to the angular vertex distributions of the three proton polyhedra hexadedron (cube), icosahedron, and dodecahedron (Figures 1D, 1D', and 1D", respeotively) taken together [where vertices labeled *h* (holes) are excluded; see text]. The same is true for insert 2 (which differs from insert 1 only in orientation) and the neutron polyhedra in Figures 1e, 1e', and 1e". Also, the angular vertex distribution of the imaginary dodecahedron made of the centers of all triangular faces of the rhomb-icosi-dodeca-hedron in Figure 1f' is analyzed into the angular distribution of dodecahedral vertices occupied by sets of three neutrons (Figure 1f') and the angular distribution of dodecahedral vertices (see letters *h* in Figure 1f') forming an hexahedron (cube; Figure 1f). Even similar polyhedra in the figure (with the exception of the cubes) have different angular vertex distributions, since they have different orientations. The occupied polyhedral vertices stand for most probable positions of nucleons presented by hard spheres of definite sizes ($r_n = 0.974$ fm and $r_p = 0.860$ fm). All polyhedra of the figure of the figure are considered superimposed with a common center and relative orientations as shown, which bring the "hard spheres" of each proton (neutron) shell in contact with the "hard spheres" of the previous and of the next proton or neutron shell. For the derivation of the cumulative proton number $Z = 50^*$ see text.

because of the successes of the IM (Sections 3 and 4) wherever it has been applied. What should be stressed here is that the hypothesis concerning the equilibrium of nucleons considered on spheres leads *uniquely* to equilibrium polyhedra (Leech, 1957)[4] (see Appendix A) whose vertices represent the most probable positions of nucleons. The space arrangement of equilibrium polyhedral vertices corresponds to the minimization of the "mutual repulsion" components of the real nucleon–nucleon interaction including the Coulomb force.

We should like to emphasize yet again that, according to the IM, the nucleons are in constant motion and that the relative positions of the nucleons (polyhedral vertices) shown in Figure 1 refer to a particular instant in time which presumably gives the average values. The periods of motion are such that the same relative positions recur after a fixed time interval. What the vertices of a polyhedron actually represent are the most probable positions of the nucleons due to their *mutual repulsion.* This repulsion ensures regions of maximum probability disposed over the surface of each shell. The mutual separation of these regions of maximum probability depends on the number of particles in the shell and *not* on the hard-core radius of the nucleon–nucleon interaction (Anagnostatos and Panos, 1982), which is substantially less than these mean separations.

We turn now to assumption (b). In order for the physical significance of the close packing[5] of shells to be understood, we employ an effective two-nucleon potential. As such a potential we take the one introduced in Anagnostatos and Panos (1982), which is reproduced in Figure 2. In this figure two hard spheres representing two nucleons in contact (with the one in the origin of coordinates) are shown. Obviously, the minimum two-nucleon separation corresponds to the case of two protons since according to assumption (b) protons are depicted by smaller hard spheres than neutrons. It is clear now from Figure 2 that even for this minimum separation we have attraction between the two nucleons. That is, this minimum separation (1.720 fm) is larger than the radius r_m (1.21885 fm) where the two-nucleon potential takes its minimum value. Therefore, since the repulsive part of the *effective* two-body potential never participates in the ground state

[4]In the α-cluster model (Margenau, 1941) the clusters are associated with the vertices of particular solids. Some of these solids may constitute equilibrium forms, but this equilibrium refers to *clusters* whereas the IM considers equilibrium of *neutrons* and *protons*, which makes the IM essentially different from the α-cluster model.

[5]It is important to make a distinction between the concept of the close packing of nuclear shells as introduced and applied in this paper and the concept of close packing as utilized in the polyspheron theory (Pauling, 1965a). Indeed, in that theory the idea of close packing refers to the close packing of spherons making up the nucleus, a spheron being an aggregate of 0 to 2 neutrons and (or) 0 to 2 protons in all possible combinations.

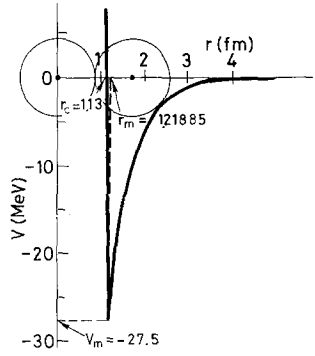

Fig. 2. Effective two-nucleon potential V versus separation distance r. The core radius of V is denoted by r_c, while the value of r where V takes its minimum value V_m is denoted by r_m. The two circles represent the hard spheres of two protons ($r_p = 0.860$ fm) in contact, one of which is at the origin.

nucleon interaction, the least energy of the nuclear system, as far as the attractive part of the nuclear force is concerned, corresponds to the *least* distances among nucleons, given of course that the nuclear shells retain their polyhedral dynamic shapes by assumption (a). Consequently, the minimum separation among all nucleons of a shell is achieved when the radius of the shell attains its minimum value. This minimum value is obtained, with the exception of the first shell (whose nucleons really are in contact), through the contact of nucleons of *successive* shells, i.e., when the nucleons of a shell come in contact with those of the previous shell, it being either a proton or a neutron shell. In other words, the nucleons of a shell (excepting the first) cannot touch each other, because such a contact would mean an even smaller shell radius, which leads to overlapping of the hard spheres of the nucleons of the shell with those of the previous one, contrary to assumption (b).

2.2. Principles

Besides assumptions (a) and (b) we use in the course of the development of the IM the following generally accepted physical principles:

(α) Identical particles in a shell are interchangeable (indistinguishable).

(β) According to quantum mechanics the wave function has the basic property of parity, i.e., $\psi(\bar{r}) = \pm\psi(-\bar{r})$. From this we conclude that $\psi^2(\bar{r}) = \psi^2(-\bar{r})$ for all $\bar{r}$ and, hence, also for the $\bar{r}$ corresponding to the most probable position. Therefore for each particle at the most probable position there exists its central symmetric counterpart.

(γ) Under the concept nuclear shell we understand a saturated structure in the sense that any addition of particles (which implies exertion of forces

between the added particles and the particles already in the shell) is impossible in that shell. Any new particles must begin a new shell.

2.3. The Possible Instantaneous Angular Distributions of the Particles in the IM

According to Leech (1957) concerning particles of the same kind on a sphere, there are only certain configurations in which these particles are in equilibrium regardless of the specific law of force among the particles. In particular, the only such configurations are the following two sets of configurations:

(A) Those in which the particles are equally spaced on a great circle, with or without two additional particles, one at each pole.

(B) Those which, in relation to a high-symmetry polyhedron (inscribed in the sphere), comprise a set of particles at its vertices or a set at the midpoints of its edges or a set at the centers of its faces or any two or all there of these sets taken together. All these high-symmetry polyhedra [namely, the zerohedron (0-h), tetrahedron (4-h), hexahedron (6-h), octahedron (8-h), cubeoctahedron (6-8-h), dodecahedron (12-h), icosahedron (20-h), icosidodecahedron (20-12-h), rhombic dodecahedron (r-12-h), rhombic triacontahedron (r-30-h)], hereafter called equilibrium polyhedra, are shown and discussed in Appendix A, (Figure 4, rows 1 and 2). Among the three possible positions (vertices, midpoints of edges, centers of faces) for identical particles with respect to a polyhedron we take the vertices. We may do so without any loss of generality, since by taking the midpoints of edges or the centers of faces, we generate a polyhedron which is again an equilibrium polyhedron, while taking any two or all three of these three possible positions is equivalent to taking two or three of the equilibrium polyhedra in the appropriate orientation (i.e., vertices of the one correspond to the midpoints of edges or to the centers of faces of the other). Thus, all configurations of Leech's type (B) are essentially the configurations of the vertices of the ten equilibrium polyhedra given in Appendix A, Figure 4, rows 1 and 2, which can be used more than one time.

In the following by utilizing principles (α)-(γ) we shall exclude from configurations (A) and (B) certain configurations. Indeed, out of the equilibrium configurations (A) (excluding plane configurations on a great circle) only the zerohedron (resulting from the two poles themselves) and the octahedron (resulting from a square in a great circle plus two poles) obey principle (α), which requires indistinguishability of particles, which in the model means indistinguishability of polyhedral vertices. Both these polyhedra belong also to configurations (B). In all other three-dimensional configurations of set (A) each pole has a different number of neighbor vertices from those corresponding to each of the vertices of the regular

polygon on the great circle and thus it is distinguishable from them. Both these polyhedra belong also to configurations (B). Also from configurations (B) the r-12-h and r-30-h are excluded as having two types of vertices A and B with different numbers of neighbors, which makes them distinguishable (Figure 4). It should be noted that r-12-h and r-30-h are excluded *as they stand*, but they can be analyzed into the two-member polyhedra, that is the r-12-h into a cube and an 8-h, and the r-30-h into a 12-h and a 20-h, which taken together have the same angular distribution as the two initial polyhedra r-12-h and r-30-h, respectively. Further, out of the equilibrium polyhedra of Figure 4, rows 1 and 2, the 4-h is the only one not obeying principle (B) and is therefore also excluded (since each vertex of this polyhedron does not have its central symmetric counterpart). Finally, the 6-8-h is excluded because it does not satisfy principle (γ), since any addition of particles may cause transformation of this polyhedron into the more symmetric (stable equilibrium) 20-h which has the same number of vertices. The r-12-h (even analyzed into an 8-h and a 6-h) is now excluded since its reciprocal (Coxeter, 1963) 6-8-h is excluded from above.

Thus, applying assumption (a) and principles (α)-(γ) we are left with seven equilibrium polyhedra, namely, the 0-h, 6-h, 8-h, 12-h, 20-h, 20-12-h, and the "r-30-h" (when considered analyzed into two polyhedra). All these polyhedra form the following reciprocal (Coxeter, 1963) (Appendix A) pairs: 0-h and 0-h, 8-h and 6-h, 20-h and 12-h, 20-12-h and "r-30-h"; these pairs can be considered as possible representations of the instantaneous dynamic shapes of nuclear shells.

Now we invoke Leech's article (1957) once more and consider the equilibrium of two *different* kinds (sets) of particles on the same sphere, in our case of neutrons and protons, whatever the law of force may be between particles of any one set and whatever else it may be between particles of the two sets. In such a case each set of particles must be in equilibrium by itself, that is, it must form an equilibrium polyhedron, and the relative orientation of the two equilibrium polyhedra must be such that the vertices of the one correspond to the middle of edges or to the center of faces of the other. As will become obvious in Section 2.4 assumption (b) leads to the center of faces. Thus, for a given neutron (proton) polyhedron the kind and orientation of the proton (neutron) polyhedron is fixed. These polyhedra are called reciprocal to each other (Appendix A), that is their axes of symmetry coincide; if, for example, an 8-h (or a 20-h) is a neutron polyhedron, its reciprocal, the cube, (or the 12-h) stands for the proton polyhedron.

We finally consider sets of particles, of one or two kinds, on different (two or more) spheres. It is obvious that in order for all the particles to be in equilibrium, each set on its sphere must be in equilibrium and also the sets on the different spheres must be in equilibrium with each other. Hence,

each configuration on its sphere must have a polyhedral form and the relative orientation among these polyhedra must be such that their common axes of symmetry coincide, which means that the vertices of each one correspond to center of faces of any of the others. Consequently, assumption (α) almost by itself yields the possible instantaneous angular distributions of neutrons and protons in the IM. We should note at this point that any order of succession of these polyhedra is acceptable up to this stage. This order, nevertheless, is restricted by virtue of assumption (β), as we shall set out in Section 2.4. For more details on the relative orientation of the polyhedra employed by the model as presented in Figure 1 one can refer to Appendix B.

2.4. The Radial Instantaneous Distribution of the Particles in the IM

Since the possible instantaneous angular distributions of the nucleons have already been established, we proceed to derive the radial instantaneous distribution of the particles by taking into account assumption (β). In other words, the size of each polyhedron takes its minimum value in such a way that the hard spheres representing the neutrons or protons of this polyhedron come in contact with those of the previous polyhedron in the angular distribution considered. In order to obtain the close packing of polyhedra it is clear that we must start with the polyhedron possessing the smallest number of particles (vertices). Therefore, we must start with the 0-h then with the 6-h and 8-h, the 12-h and 20-h, and so forth. Since we have two kinds of particles which according to Leech (1957) occupy reciprocal polyhedra, one of the members of a reciprocal pair is assigned to neutrons and the other to protons. We found it workable in the model to start by assigning the neutrons to stable equilibrium polyhedra (i.e., 8-h, 20-h, etc.) and the protons to the unstable equilibrium polyhedra (i.e., 6-h, 12-h etc.) which acquire stability when considered together with their reciprocal (see Appendix A). After a very detailed and tedious examination of all possibilities we have arrived at the instantaneous dynamic forms of all nuclear shells and their close packing as shown in Figure 1, which demonstrates the sizes and the relative orientations among neutron polyhedra, among proton polyhedra, and among neutron and proton polyhedra.

As one can see from Figure 1 the close packing of shells leads to the creation of holes (denoted by h) in some polyhedra and to the analysis of some polyhedra into simpler ones (where possible). For an explanation of both one can consult Appendix E.

The polyhedra standing for proton shells lie on the left of the heavy central vertical line in Figure 1, while those for neutrons are on the right

and in such a correspondence that next to a proton (neutron) polyhedron (in each of the levels of the figure which are labeled A–F for protons and a–f for neutrons) one finds a neutron (proton) polyhedron having the same symmetry group (i.e., reciprocal in geometrical language). In levels D and E of Figure 1, the angular vertex distribution of the proton or neutron rhombic triacontahedron (see inserts 1 and 2 in Figure 1) is analyzed into three simpler equilibrium polyhedra (standing for nuclear subshells). A somewhat more sophisticated analysis into polyhedral subshells is made for the last neutron shell (see Figures 1f and 1f'). In this case for a better visualization, we consider the centers of the triangular faces of the rhombicosidodecahedron which form an imaginary dodecahedron each vertex of which stands for a set of three vertices of the initial polyhedron. With these in mind, the polyhedra in Figures 1f and 1f' can be visualized, for example, like those in Figures 1e and 1e'. Finally, for the polyhedra of Figure 1 we may say that if the similar polyhedra in levels D and E of the figure (and in inserts 1 and 2) are considered different, because of their different orientation, then all polyhedra in Figure 1 are different in the sense that their angular vertex distributions are different.

At the top of each block in Figure 1 the name of the polyhedron presented there is given, while at the bottom the number of succession of the subshell (having this polyhedron as its instantaneous dynamic average form) is shown inside a box with the prefix Z for protons and N for neutrons. Underneath this box, the number of vertices of the polyhedron and the number of holes (h, if any) (whose difference is the number of nucleon most probable positions accommodated by this polyhedron) are given inside parentheses, while next to it inside brackets the cumulative number of nucleon most probable positions, accommodated by all previous polyhedra, is given. Finally, in each block, the size of the sphere exscribed to this polyhedron is given in units of fermis.

The information needed for the reproduction of all radial sizes of the nuclear shells, completely determined from the hard spheres of neutrons and protons and from the angular distribution of polyhedral vertices, is given in Appendices C and D. The calculation starts from the 0-h and proceeds step by step leading to the radii of the spheres exscribed to all polyhedra of Figure 1.

It is apparent that the instantaneous dynamic structure of the IM is now metrically defined. Thus, the coordinates of all nucleon most probable positions, involved in a particular closed shell nucleus, can be uniquely determined. For example, these coordinates for the doubly closed-shell nuclei ^{4}He, ^{16}O, and ^{40}Ca are given in Footnote 14 of Anagnostatos and Panos (1982).

3. APPLICATIONS OF THE IM

3.1. Reproduction of Magic Numbers

As one can see, the cumulative numbers in the brackets of Figure 1 reproduce all experimentally known magic numbers (we will comment on the derivation of $Z = 50$ shortly). In addition, for protons the semimagic numbers at $Z = 28$ and 40 are reproduced, while for neutrons the numbers $N = 58$, 70, and 90 appear, which are meaningful also. Specifically, $N = 58$ and 70 correspond to closures of subshells, according to the order of levels following the single-particle shell model (Mayer and Jensen, 1955), while $N = 90$ (even though not in this order) corresponds to a closure of a subshell, according to the experimental data (Holden and Walker, 1972) (since after $N = 82$ the $2f_{\frac{7}{2}}$ states appear (i.e., totally 8 neutrons) in the ground states of odd N even Z nuclei).

It is interesting to comment that the number $Z = 52$, instead of $Z = 50$, results from the summation of all proton most probable positions up to Figure 1D″. This fact, as will be explained in detail elsewhere, forms the starting point for an explanation of the rarely seen magic number $Z = 50$ in the low-energy fission products of ^{235}U and in spallation procedures. The magic number $Z = 50$ is here explained as follows. As one can see, there are two holes in the hexahedron of the $Z2$ which lie on the same rays with two holes of the $Z3$ shell. This creates a favorable condition for the two protons in the $Z4$ (lying on the same rays) to shrink and thus to come in contact with the protons in $Z1$. Then, in the thus-created holes in $Z4$, two additional protons could be accommodated and thus the cumulative proton number $Z = 42$ could appear. If now eight additional protons forming a cube are considered, the magic number $Z = 50$ appears. When additional protons are added, however, this structure does not remain as a core, but instead changes into that of Figure 1D″ with cumulative proton number $Z = 52$.

3.2. Radii and Densities

In Table I the results of nuclear size and density calculations (of closed-shell nuclei from ^{4}He to ^{208}Pd, *solely* based on the radial size information given in Figure 1) are presented. Specifically, the charge, neutron, proton, and neutron–proton root mean square radii (i.e., $\langle r^2\rangle_{\text{ch}}^{1/2}$, $\langle r^2\rangle_n^{1/2}$, $\langle r^2\rangle_p^{1/2}$, and $\langle r^2\rangle_n^{1/2} - \langle r^2\rangle_p^{1/2}$, the average nuclear densities, and the radial parameter r_0 of all closed-shell nuclei listed in the first column are given together with experimental or adopted values (de Jager et al., 1974; Engfer et al., 1974; Stock, 1976; Alkhazov et al., 1976; Pyle and Greenless, 1969; Greenless et al., 1970; Bernstein and Seidler, 1972; Jackson, 1976; Hornyak,

Table I. Isomorphic Model (IM), Experimental (EXP) and Spherical Shell Model (SSM) Charge, Neutron, Proton, and Neutron–Proton Root Mean Square Radii (i.e., $\langle r^2\rangle_{ch}^{1/2}$, $\langle r^2\rangle_n^{1/2}$, $\langle r^2\rangle_p^{1/2}$, and $\langle r^2\rangle_n^{1/2}-\langle r^2\rangle_p^{1/2}$ in fm, Respectively), Average Nuclear Densities (i.e., $\bar{d}$ in Nucleons/fm^2), and Radial Parameter r_0 [in fm/(nucleon)$^{1/3}$] of Closed-Shell Nuclei

Closed-shell nuclei	$\langle r^2\rangle_{ch}^{1/2}$			$\langle r^2\rangle_n^{1/2}$		$\langle r^2\rangle_p^{1/2}$		$\langle r^2\rangle_n^{1/2}-\langle r^2\rangle_p^{1/2}$			$\bar{d}$	r_0
	IM	EXP	SSM	IM	SSM	IM	SSM	IM	EXP	SSM	IM	IM
^{4}He	1.71	1.71 (4)[a]		0.97		1.55		−0.58			0.111	1.29
^{16}O	2.44	2.61 (14)[b]	2.69	2.23	2.55	2.33	2.59	−0.10		−0.04	0.119	1.26
^{40}Ca	3.47	3.482 (25)[a]	3.46	3.10	3.36	3.39	3.38	−0.29	−0.03[c,d]	−0.02	0.115	1.28
^{48}Ca	3.46	3.470[a]		3.51		3.39		0.12	0.12[d]		0.115	1.27
^{58}Ni	3.73	3.74[e]	3.94	3.84	3.84	3.66	3.87	0.18	0.18[f]	−0.03	0.111	1.29
^{90}Zr	4.32	4.25 (7)[a]	4.32	4.35	4.29	4.26	4.18	0.09	0.16 (9)[g]	0.11	0.117	1.27
^{120}Sn	4.63	4.630 (7)[b]	4.73	5.07	4.73	4.58	4.56	0.49	0.49 (19)[h]	0.17	0.109	1.30
^{142}Nd	5.03	4.993 (35)[a]	4.97	5.41	4.96	4.98	4.84	0.43		0.12	0.105	1.31
^{208}Pb	5.58	5.521 (29)[a]	5.62	6.50	5.64	5.54	5.45	0.96	0.64 (26)[h]	0.19	0.096	1.35
											$\bar{d}=0.111$	$\bar{r}_0=1.29$
								adopted values[i]			$\bar{d}=0.113$	$\bar{r}_0=1.25$

[a] See de Jager et al. (1974).
[b] See Engfer et al. (1974).
[c] See Stock (1976).
[d] See Alkhazov et al. (1976).
[e] See Pyle and Greenless (1969).
[f] See Greenless et al. (1970).
[g] See Bernstein and Seidler (1972).
[h] See Jackson (1976).
[i] See Hornyak (1975).

1975) for comparison. For comparison with theoretical predictions, other than those included in the table and discussed later, see Hodgson (1980) and references therein. For the calculations involved, the definition of each quantity as given below is used:

$$\langle r^2\rangle_{\rm ch}^{1/2} \equiv \left[\frac{\sum_{i=1}^{Z} r_i^2 + Z(0.8)^2 - N(0.34)^2}{Z}\right]^{1/2} \tag{2}$$

$$\langle r^2\rangle_n^{1/2} - \langle r^2\rangle_p^{1/2} \equiv \Delta r_{np} \equiv \left(\frac{\sum_{i=1}^{N} r_i^2}{N}\right)^{1/2} - \left(\frac{\sum_{i=1}^{Z} r_i^2}{Z}\right)^{1/2} \tag{3}$$

$$d = \frac{A}{(4/3)\pi R_{\rm eq}^3}$$

$$R_{\rm eq} = (5/3)^{1/2}\langle r^2\rangle^{1/2} \tag{4}$$

$$\langle r^2\rangle_{\rm mass}^{1/2} = \left[\frac{\sum_{i=1}^{A} r_i^2 + Z(0.860)^2 + N(0.974)^2}{A}\right]^{1/2}$$

and

$$r_0 = [(4\pi/3)d]^{-1/3} \tag{5}$$

where Z, N, and A are the proton, neutron, and mass numbers, respectively; 0.8 fm ($-0.116\,\text{fm}^2$) stands for the charge rms radius (ms) of a proton (Engfer *et al.*, 1974) (neutron); 0.860 fm (0.974 fm) stands for the mass rms radius of a proton (neutron), according to the isomorphic model [assumption (b)]; and r_i stands for the distance of the ith neutron or proton center from the nuclear center, as given by the relevant R value in Figure 1.

As is obvious from Table I the comparisons of the model predictions with the experimental or adopted values (where available) are very satisfactory. Specifically, the model charge rms radii are either within the ranges defined by the experimental errors, or when out of it, no more than $3(10^{-2})$ fm. This accuracy is very good, particularly because, first, no adjustable parameters are used in the calculations and, second, everything in Table I comes uniquely from a structural rule (followed consistently from ^{4}He to ^{208}Pb) and from the definitions of the estimated quantities. As for the neutron-proton rms radial differences there is insufficient information in the literature. Specifically, data for some nuclei in Table I are missing and where available they come from different sources and methods. As is

known, different methods applied to the same nucleus may give substantially different results. In general, the experimental knowledge of neutron distribution is very vague and has been marked by some confusion and controversy. It depends rather strongly on the choice of the nucleon-nucleon interaction and of other strongly interacting projectiles during scattering and reaction procedures (Jackson, 1976). The way of deriving the neutron distribution here, however, lends support to our predictions, since both proton and neutron distributions are interconnected and both come from the same structural role of close packing of reciprocal equilibrium polyhedral shells, as illustrated in Figure 1. Thus, it is reasonable to believe that the neutron distribution is as reliable as the proton distribution, when the latter fits the experimental data for the radii and Coulomb energies (Anagnostatos and Panos, 1982) very well.

A very interesting feature of our results is that the Nolen-Schiffer effect (Nolen and Schiffer, 1969) for calcium isotopes (i.e., the charge radius of ^{48}Ca is smaller than that of ^{40}Ca) is well reproduced. This is a consequence of equation (2), which includes the effect of neutron charge density (Bertozzi et al., 1972). Also, our Δr_{np} values and their change of sign for these two calcium isotopes are very well justified by the experimental data, while these values and the Nolen-Schiffer effect are in apparent conflict with Hartree-Fock predictions.

The average values of density and of radial parameter r_0 for all nine nuclei of Table I, i.e., $\bar{d}_A = 0.111$ nucleons/fm^3 and $\bar{r}_0 = 1.29$ fm, compare very well with the adopted values $d_A = 0.113$ nucleons/(fm^3) and $r_0 = 1.25$ fm for all nuclides, when a trapezoidal-density function is assumed (Hornyak, 1975).

Since for each closed-shell nucleus all previous closed shells coexist as a core (in the isomorphic model), the derived densities in Table I constitute an approximation (for pointlike nucleons) of the radial dependence of density. The deviations from their average value remind one of the experimentally and theoretically known waving radial fluctuations of density (Negele, 1976). The rather significant decrease of density after ^{90}Zr resembles the decrease in binding energy per particle as a function of A for this mass region (Kaplan, 1962). That is, our decrease in density gives an explanation of the decrease in binding energy, in cooperation with the increase of Coulomb energy as Z increases, and offers an additional support for our calculations. Of course, this decrease in density comes almost exclusively from the size of our $N9$ radius (see Figure 1f'), which leads to Δr_{np} for ^{208}Pb (see Table I) higher than any available experimental information. This significant neutron halo (neutron skin) in Pb is very difficult to detect accurately, being very sensitive to the particular projectile employed (Rebel, 1976).

3.3. Coulomb, Kinetic, and Binding Energies

For this section ^{16}O and ^{40}Ca are taken as examples. The quantities involved have already been published in the references cited but are also given here for reasons of completness.

Despite the fact that the nucleons in the IM are in constant motion, all quantities are computed considering the nucleons in their most probable positions shown in Figure 1. Of course, these positions refer to a particular instant in time, but they presumably give the average values.

An estimation of the Coulomb energy, E_C, for each closed-shell nucleus can be determined by applying the Coulomb potential to all pairs of proton most probable positions (Figure 1). Such E_C values (considered as average values) for ^{16}O and ^{40}Ca are taken from Anagnostatos and Panos (1982) and are listed in Table II.

The average kinetic energy per nucleon, $\langle T \rangle$, can be determined as the sum of the part of the kinetic energy due to the confinement of the nucleons in the nuclear volume and of the part of the kinetic energy due to the rotation of nucleons (Svenne, 1980). Values of $A\langle T \rangle$ (A denoting number of nucleons) that are listed in Table II are taken from Panos and Anagnostatos (1982a, b) and (as explained there) have been computed using, as for the Coulomb energies, the same nucleon most probable positions (Figure 1).

For the determination of binding energies, BE, we use the formula

$$\mathrm{BE} = \sum_{\substack{\text{all nucleon} \\ \text{pairs}}} V_{ij} - E_C - A\langle T \rangle \tag{6}$$

Table II. Coulomb, Kinetic, and Bind Energies, in Units of MeV, for ^{16}O and ^{40}Ca

Nuclei	E_C	$A\langle T \rangle$	ΣV_{ij}	BE	Separation neutrons	Energies protons
^{16}O	12.4[a]	126[c]	255.1[e]	116.7	$1s^{1/2}$ 62.41	40.01
	(10.7-12.5)[b]	(131)[d]		(127.6)[f]	$1p^{3/2}$ 17.63	14.13
	64.8	324	757.1	368	$1p^{1/2}$ 13.73	8.53
^{40}Ca	(61.1-71.2)	(362)		(342.1)		

[a] According to the second term on the right-hand side of equation (6).

[b] According to the formula $E_C = (e^2/R^2)[0.6Z(Z-1) - 0.46Z^{4/3}]$, where $R = (1.3 \pm 0.1)A^{1/3}$, from Hill (1957).

[c] See Panos and Anagnostatos (1982a, b).

[d] According to the single-particle sum rule in Svenne (1980) and Panos and Anagnostatos (1982a, b).

[e] See Anagnostatos and Panos (1982).

[f] See Wapstra and Gove (1971).

An estimation of the potential energy, $\sum V_{ij}$, for each closed-shell nucleus can be obtained by employing the two-body potential of Figure 2 for all pairs of nucleon most probable positions (Figure 1). Such $\sum V_{ij}$ values (considered also as the average values) for our sample nuclei are taken again from Anagnostatos and Panos (1982) and are also listed in Table II. Next to them the corresponding BE are given. As one can see from Table II the quantities E_C, $A\langle T\rangle$, and BE are in very good agreement with experimental values listed also in the table. It is important that all the above quantities are calculated without any adjustable parameters. More details concerning the determination of BE will be given elsewhere.

These energy predictions are a very sensitive check of the average gross structure of these nuclei proposed by the isomorphic model. A similar check is underway for the heavier closed-shell nuclei and will be critical for a check of the dimensions of the last neutron shell, which is responsible for the rather large Δr_{np}, and thus rather small nuclear density, in ^{208}Pb.

4. COMPARISON BETWEEN THE PREDICTIONS OF THE ISOMORPHIC MODEL AND THOSE OF OTHER NUCLEAR STRUCTURE MODELS

4.1. Spherical Shell Model

4.1.1. Magic Numbers

It is worth noticing that in the explanation of magic numbers given herein lies a main difference between the isomorphic model and the shell model: In the shell model the reproduction of the magic numbers follows only if we introduce empirically a spin–orbit term in the effective interaction and, moreover, if we more or less artificially "bunch" the nucleon numbers to generate shells and subshells, which we call "closed" so as to get the experimentally known magic numbers. Specifically, while the evidence for spin–orbit coupling introduced by the shell model is convincing, it is difficult, to understand (on the basis of the arguments usually employed) why the magic numbers should be outstanding among the many more numbers corresponding to the completion of spin–orbit sub-subshells (Pauling, 1965b).

In contradiction, the explanation of magic numbers given by the isomorphic model follows a natural way. Thus, incorporating into the conventional shell model the concept of a nuclear shell introduced by the isomorphic model, one could conclude that nuclear shell structure is more general than the independent-particle basis upon which it currently rests. Specifically, the abstract concept of a shell, introduced by the shell model, in the framework of the isomorphic model is shown to lead to nuclear shells with

real shapes when one considers the most probable position of each nucleon instead of its innumerable intantaneous positions in orbital.

4.1.2. Radii and Densities

In Table I the results of nuclear radii, according to the spherical shell model (SSM) calculations, are given for comparison with those of the isomorphic model (IM). In particular, the single particle potential (SPP) method was applied in which each nucleon is moving independently in a one-body potential, and the proton and neutron density distributions are then obtained by summing their probability distributions, weighted by the occupation numbers of each orbit (Hodgson, 1981). As one-body potential the following was used:

$$V_J(r) = -V_N f(r) - \left(\frac{\hbar}{m_\pi c}\right)^2 \frac{V_{so}}{a_{so}} (\bar{L}\cdot\bar{\sigma})_J g(r) + Z_A Z_\mu e^2 h(r) + \frac{\hbar^2 L(L+1)}{2\mu r^2}$$

where

$$f(r) = \left[1+\exp\left(\frac{r-R_N}{a_N}\right)\right]^{-1},$$

$$g(r) = \frac{\exp\left(\dfrac{r-R_{so}}{a_{so}}\right)\left[1+\exp\left(\dfrac{r-R_{so}}{a_{so}}\right)\right]^{-2}}{r}$$

$$h(r) = \frac{1}{r} \qquad \text{for } r \geqslant R_c$$

$$= \frac{1}{2R_c}\left(3-\frac{r^2}{R_c^2}\right) \qquad \text{for } r < R_c$$

V_N is the central nuclear potential; V_{so} is the spin-orbit nuclear potential; and

$$(\bar{L}\cdot\bar{\sigma})_J = L \qquad \text{for } J = L+1/2$$

$$= -(L+1) \qquad \text{for } J = L-1/2$$

r_x, a_x are the radius and diffuseness parameters of the xth part of the potential and $R_x = r_x A^{1/3}$; A, Z_A are the core mass and its charge; μ, $Z\mu$ are the particle reduced mass and its charge.

In general, all the details of the method applied are included in the Oxford Computer Density Code made available to us by the Oxford Nuclear Physics Theoretical Group.

The agreement between the results of the two models is quite good, as can be seen from Table I. While there are obvious differences in the results,

overall, the two models give predictions that are quite well comparable to the experimental data, as seen from the table.

Since the nucleon distribution in the isomorphic model (as shown in Figure 1) corresponds to the momentary dynamic distribution of nucleon most probable positions, the density derived from it (see Table I) is just the average density. Thus, it is very interesting to examine how this distribution compares not only to the average value but also to the radial nuclear density, derived according to the spherical shell model. For this effort we have again used the Oxford Code. First, taking ^{16}O as an example, as single-particle separation energies we have taken the energies derived from the model when the two-body nuclear potential of Anagnostatos and Panos (1982) (see also Figure 2) was applied among all pairs of nucleons in the isomorphic nucleon distribution [Figure 1; see also footnote 14 of Anagnostatos and Panos (1982) for the nucleon coordinates], and the corresponding kinetic energies were subtracted (Table II). For these energies, we have determined from the Code the depths V_N and V_{so} of the one-body potential in equation (7) for each state, and the corresponding single-particle wave functions. The radial charge and matter densities derived by the Code using these wave functions are shown in Figure 3, together with the charge density

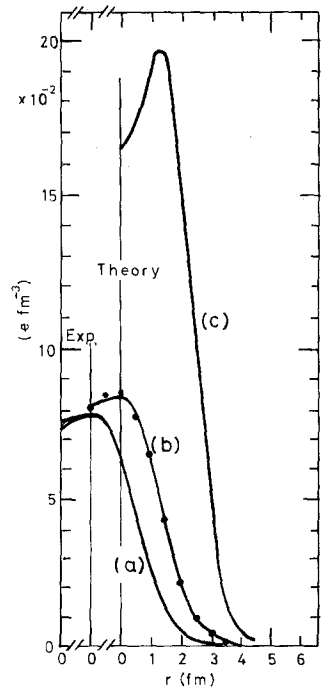

Fig. 3. Radial density distributions of ^{16}O. Part (a) represents the experimental upper and lower limits. Part (b) shows the theoretical predictions for the change density; solid curve for Brown et al. (1979), dots for this work. Part (c) shows the matter density according to the present work.

derived by "pure" shell model calculations from Brown et al. (1979). The agreement between the predictions of the two models is apparent and both compare equally well with the experimental curve. For matter distribution no experimental or theoretical densities were available.

4.1.3. Quadrupole Moments

The momentary dynamic proton distributions in the model obviously have a spherical symmetry, which leads to, as desired, electric quadrupole moments for the closed shell nuclei, $Q = 0$. Further, it is very interesting to recall, for example, Anagnostatos (1973, 1977) and Anagnostatos et al. (1980), where the quadrupole moments for all open-shell nuclei in the s-d shell are very successfully predicted, when the following assumption is made. The valence protons, that is the protons in addition to the complete core of ^{16}O (where the polyhedral shells $Z1$ and $Z2$ are complete in Figure 1), occupy vertices of the next proton polyhedral shell ($Z3$). This success constitutes a very sensitive test for the distribution of the proton most probable positions in the model. Also, we should mention that the previous assumption about the filling of a shell in the IM resembles very well the way the simple shell model arranges its valence particles into unoccupied levels.

4.1.4. $\bar{l}$, $\bar{s}$, $\bar{j}$ and $\bar{j}\bar{j}$ Quantization of Direction

While this section clearly belongs to the semiclassical part of the model, which is not the subject matter of the present work, it is very interesting to recall from Anagnostatos (1978; 1980a, b) Anagnostatos et al. (1981) and de Boer and Mang (1973) that the symmetries of the regular and quasiregular polyhedra employed in the IM to represent equilibrium dynamic forms of nuclear shells are consistent, in the level of *identity* with the symmetries of quantization of direction for the orbital, intrinsic and total angular momenta, and their projection on the quantization axis. Also, they are consistent with $\bar{j}\bar{j}$ coupling and its projection, with a symmetry description of the Independent Particle Model, and with rotational invariance of orbital-angular-momentum quantization of direction for degenerate states.

Thus, an equilibrium polyhedron employed in the IM may represent the average motion patterns of the nucleons which this polyhedron accommodates in the model. In general, the angular study of equilibrium (isomorphic) polyhedra may help the development of a fundamental theory of the atomic nucleus, just as the study of regular linear arrays of identical atomic groups led towards the complete theory of crystal structure.

4.1.5. Hartree-Fock Approach

As one can see from Table 2 Panos and Anagnostatos (1982a, b) (where the single-particle sum rule average kinetic energy per particle for a selection of self-consistent field calculations for ^{16}O is given), the kinetic energy from the isomorphic model satisfies the single particle sum rule very well, while the Hartree-Fock (HF) and Bruckner-Hartree-Fock (BHF) methods do not. The IM gives equivalent results with those coming from renormalized BHF and from density-dependent HF approaches (Svenne, 1980).

4.2. Collective Models

4.2.1. Saturation

The saturation property, that is, the fact that both average density and average binding energy per particle are approximately the same for all but the lightest nuclei, is an essential property in nuclear structure physics. It is of major importance that about constant average density results directly from our two assumptions (see Table I) and that the application of the two-body potential of Anagnostatos and Panos (1982) (Figure 2) leads to almost constant average binding energy per particle (Table II). Thus, while the model starts as an independent particle model, it comes out to incorporate features of the liquid drop model.

4.2.2. Collective Rotations

In Anagnostatos (1973; 1977) and Anagnostatos et al. (1980), using a method based on our closed-shell treatment, we have used the model, in combination with predicted ground state moment of inertia, J_0, values from the variable moment of inertia (VMI) model (Mariscotti et al., 1969), to estimate the specific rotating and nonrotating part in a rotating nucleus. The model predicts that in a rotating nucleus, in general, only a part of the mass rotates and thus contributes to its J_0. Specifically, through the 78 nuclei examined we have found that this mass is not arbitrary but is related to the shell structure of the nucleus (Trainor and Gupta, 1971). Namely, this rotating mass consists either of the mass of nucleons of the incomplete shells alone, or of the mass of the incomplete shells plus the mass of an integral number of deformed closed shells in successive order for outermost to innermost.

4.2.3. Giant Resonances

Collective time-dependent relative neutron to proton movements, as in giant resonances (Bertsch, 1983), are very well qualitatively understood

in the model, where neutrons and protons form different shells. Particularly, the monopole (breathing) and quadrupole modes of vibrations are favored by the isomorphic nuclear shell structure. The small percent of nucleons participating in quadrupole vibration could be associated with the nucleons of a polyhedral shell.

4.3. Quark Model of Nucleons

It is tempting to relate the radii of the proton (0.860 fm) and neutron (0.974 fm) "hard" spheres as required in the isomorphic model with the radii of the MIT nucleon cloudy bags. Recently (Thébêrge and Thomas, 1983), these bags range between 0.8 and 1.1 fm, while another recent study (Thomas, 1983) estimates the bag radius to be 0.87 ± 0.10 fm. Furthermore, in the IM the radius of the neutron bag is 13% larger than that of the proton bag, which agrees very well with a finding (Celenza and Shakin, 1983) that in the quark model the confinement radius for a neutron is about 10% larger than for a proton. This agreement, seemingly not accidental, indicates that in the IM of nuclear ground states we may see some nucleon confinement spheres of radii similar to those found in quark models of nucleons.

5. SUMMARY AND CONCLUSIONS

In the classical part of the isomorphic model presented in this paper a rather simple structural rule is underlined, where nuclear shells with instantaneous dynamic average forms represented by reciprocal equilibrium polyhedra (whose vertices stand for nucleon most probable position and are occupied by hard spheres of definite sizes) are packed in the closest way. From this part alone the experimentally known magic numbers are reproduced in a unique way. Charge, neutron, proton (and their difference) rms radii, average and radial nuclear densities, Coulomb energies, kinetic and binding energies of closed-shell nuclei are also derived in very good agreement with experimental data and using no adjustable parameters, even though some more work seems necessary for a check of the sizes of the heavier shells. In Section 4 of this paper a first comparison of the IM with other nuclear structure models (that is, the spherical shell model, collective models, and the quark model of nucleons) shows that while the model starts with the nuclear shells, i.e., in the lines of the independent particle model, it finally leads to sizes, densities, Coulomb and binding energies consistent with the liquid drop model, using sizes of nucleons consistent with the quark model of nucleons. Specifically, it can be argued that our assumption

(a) is along the lines of the independent particle model, while our assumption (b) links the isomorphic model to the liquid drop and quark models.

Finally, we would like to stress once more that the IM should *not* be seen as a competitor to any of the existing nuclear structure models but rather as a link among them. There is not a real difference in physics between the IM and the other models but rather differences in the approaches employed. Further work on the IM may prove very useful by contributing a great deal to the formation of a "picture" of the nucleus which can unite the available information about nuclei into a consistent body of knowledge.

ACKNOWLEDGMENTS

I am particularly indebted to Dr. G. Flessas of Glasgow University for a very critical reading of the manuscript and constructive criticism. Also, I want to thank Dr. S. E. Massen of the University of Salonica for his help in the spherical shell model calculations using the Oxford Computer Density Code and Mr. Ph. Trouposkiades for his painstaking and careful work in making the drawings.

APPENDIX A: CLASSIFICATION OF EQUILIBRIUM POLYHEDRA

In this appendix we discuss all ten different equilibrium polyhedra which are illustrated in Figure 4, rows 1 and 2, along with their names and their symbolic abbreviations. Some important classifications of these polyhedra are as follows:

(i) All ten polyhedra are divided into two sets according to their regularity. The tetrahedron, hexahedron, octahedron, dodecahedron, and icosahedron comprise all the Platonic (regular) polyhedra. The zerohedron is considered as the degeneration of a regular polyhedron to zero dimensions. The remaining four semiregular polyhedra, namely, the rhombic dodecahedron, cuboctahedron, rhombic triacontahedron, and icosidodecahedron, may be derived from the Platonic polyhedra in the following ways. When we consider a hexahedron and an octahedron with mutually bisecting edges (Figure 4, row 3, column 3), then their vertices taken together are the vertices of a rhombic dodecahedron, and their common volume has the shape of a cuboctahedron. Similarly, when we consider an icosahedron and a dodecahedron with mutually bisecting edges (row 3, column 5), then their vertices taken together are the vertices of the rhombic triacontahedron and their common volume has the shape of an icosidodecahedron.

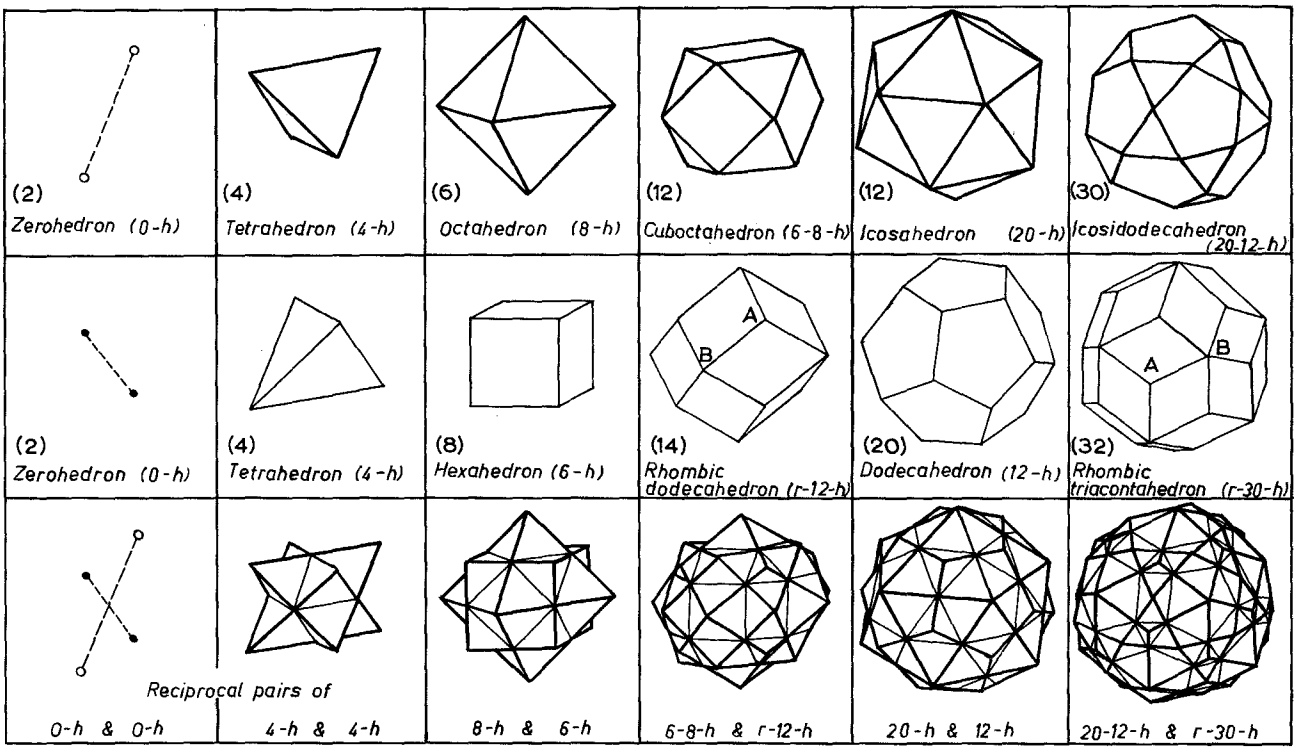

Fig. 4. Equilibrium polyhedra representing configurations of particles in equilibrium on a sphere independent of the actual laws of forces among particles. Polyhedra in the first two rows of each column are reciprocal, i.e., the vertices of the one correspond to the center of faces of the other. As shown in the last row, their corresponding edges are taken to intersect each other at right angles when the two polyhedra are combined. Inside parentheses our symbolic abbreviations for the polyhedral names are given. A and B distinguish between two kinds of vertices, each possessing a different number of neighboring vertices. In each block inside parentheses the number of vertices of the relevent polyhedron is given.

The hexahedron, octahedron, cuboctahedron, rhombic dodecahedron, and the dodecahedron, icosahedron, icosidodecahedron, rhombic triacontahedron, belong to the cubic-octahedral and the icosahedral-dodecahedral symmetry group, respectively.

(ii) All ten polyhedra of Figure 4, rows 1 and 2, can be divided into pairs of reciprocal polyhedra (Coxeter, 1963). In short, two polyhedra are reciprocal (dual) when the radii passing through the vertices of one, cross the faces of the other perpendicularly at their centers (Coexter, 1963, p. 17). Accordingly, as shown in column 1 of Figure 4, the zerohedron has another zerohedron as its reciprocal, i.e., it is self-reciprocal. Likewise, the tetrahedron is self-reciprocal. In addition the following pairs of polyhedra appropriately oriented, are reciprocal: the octahedron and hexahedron, the cuboctahedron and rhombic dodecahedron, the icosahedron and dodecahedron, and the icosidodecahedron and rhombic triacontahedron. Each column in Figure 4 contains one of these reciprocal pairs, first (rows 1 and 2) with the members shown separately, and then (row 3) superposed in the appropriate manner.

(iii) All ten polyhedra can be divided into two sets according to their stability, i.e., stable or unstable equilibrium of particles considered at their vertices. Stable equilibrium in geometrical language means that the distance between any two neighboring particles (least distance) must be the maximum possible. Thus the zerohedron, tetrahedron, octahedron, icosahedron, and icosidodecahedron satisfy this condition. The remaining polyhedra do not fulfill this condition. For example, while eight particles on a sphere are at equilibrium at the vertices of a cube, they do *not* have a maximum least distance; this least distance becomes maximum when the 8 particles are arranged at the vertices of a square antiprism which, of course, is *not* an equilibrium polyhedron.

(iv) All ten polyhedra can be divided into two sets according to their central symmetry. Only the tetrahedron does not possess this symmetry, since the central reflection of a vertex of the tetrahedron does not correspond to another vertex of this polyhedron.

(v) All ten polyhedra can be divided into two sets, according to whether the number of nearest neighbors of each particle (vertex) is the same or not. From the polyhedra of Figure 4 only the rhombic dodecahedron and the rhombic triacontahedron have two categories of vertices A and B. Specifically, in the rhombic dodecahedron each vertex A has four neighbor vertices and each vertex B three neighbor vertices, while in the rhombic triacontahedron each vertex A has three neighbor vertices and each vertex B five neighbor vertices.

Table III describes all the metrical relationships of the regular polyhedra and comes from Coxeter (1963), p. 292.

Table III. Metric Characteristics[a] of the Kinds of Polyhedra used in the Model

Column: 1	2	3	4	5	6	7	8	9	10
Polyhedron	Number of			Characteristic polyhedral angles			Radii (R) with respect to length of half-edges (L)		
	Vertices	Edges	Faces	$\hat{\phi}^b$	$\hat{\chi}^b$	$\hat{\psi}^b$	Of exscribed sphere, $0^{R/L}$	Of middle sphere, $1^{R/L}$	Of inscribed sphere, $2^{R/L}$
Zerohedron	2	—	—				1.0000	—	—
Octahedron	6	12	8	45° 0′ 0″	54° 44′ 8″	35° 15′ 52″	1.4142	1.0000	0.8165
Hexahedron[a]	8		6	35° 15′ 52″		45° 0′ 0″	1.7321	1.4142	1.0000
Icosahedron	12	30	20	31° 43′ 3″	37° 22′ 38″	20° 54′ 19″	1.9020	1.6180	1.5115
Dodecahedron	20		12	20° 54′ 19″		31° 43′ 3″	2.8026	2.6180	2.2271
Icosidodecahedron	30	60	32		31° 43′ 3″		3.2361	3.0779	2.9274
Rhombic triacontahedron	32		30					1.4472	

[a] Not all the characteristics listed are used in the paper, but they are given for reasons of completeness and future applications and are taken from Coxeter (1963).

[b] If we denote by 0 a vertex, by 1 the middle of an edge, by 2 the center of a face, and by 3 the center of a polyhedron, then $\hat{\varphi} = 0\hat{3}1$, $\hat{\chi} = 0\hat{3}2$, and $\hat{\psi} = 1\hat{3}2$ (see Coxeter, 1963).

APPENDIX B: RELATIVE ORIENTATIONS OF EQUILIBRIUM POLYHEDRAL SHELLS

This appendix describes in detail the relative orientation of all polyhedra employed by the isomorphic model, as shown in Figure 1.

The neutron zerohedron ($N1$) is the first neutron polyhedron involved in the isomorphic nuclear structure. Its two spheres representing its two neutrons are in contact, as assumption (b) requires. Their point of contact defines the nuclear center, which is the center of symmetry as well, and the straight line through their centers defines an axes of symmetry. The first proton polyhedron (the zerohedron $Z1$) has the same center of symmetry as $N1$, but its two spheres representing its two protons cannot be in contact with each other) since then the spheres of the two protons and of the two neutrons would overlap one another, which is not possible since the spheres are assumed "hard"), and their separation distance is defined by the contact of each proton sphere with the neutron spheres of $N1$. The straight line through the centers of the two proton spheres defines another axis of symmetry. This axis of $Z1$ and the previous axis of $N1$ are perpendicular and common axes of symmetry of both $N1$ and $Z1$, and cross each other at the common center of symmetry, the nuclear center.

The next smallest polyhedra involved in the isomorphic nuclear structure are the octahedron $N2$ and the hexahedron $Z1$. Their orientation with respect to $N1$ and $Z1$ and between themselves is such that the n–n and p–p axes of symmetry of $N1$ and $Z1$ become $C2$ and $C3$ axes, respectively, of both the $N2$ and $Z2$. It is interesting for one to notice that in this orientation $N2$ and $Z2$ have all their $C2$, $C3$, and $C4$ symmetry axes common, i.e., they have a common rotational group, or they are reciprocal in geometrical language.

Next in the isomorphic structure come the polyhedra with larger numbers of vertices, i.e., the icosahedron ($N3$) and the dodecahedron ($Z3$). Their orientation to all four previous polyhedra and between themselves is in such a way that all $C3$ axes of $N2$ and $Z2$ are $C3$ axes of both $N3$ and $Z3$ and in addition all $C4$ axes of $N2$ and $Z2$ are $C2$ axes of both $N3$ and $Z3$. At the same time, all $C2$, $C3$, and $C5$ symmetry axes of $N3$ and $Z3$ are common, i.e., these two polyhedra constitute a reciprocal polyhedral pair.

Finally, the largest equilibrium polyhedra are considered, i.e., the icosidodecahedron ($N4$) and the rhombic triancontahedcron (insert 1). The rotational group of each of these two polyhedra is the icosahedral-dodecahedral group, i.e., these two polyhedra are reciprocal. Thus, their orientation to each other is such that their symmetry axes coincide and, at the same time, all these axes coincide with all symmetry axes of $N3$ and

$Z3$. In Figure 1 this rhombic triancontahedron for close packing requirements is analyzed into three polyhedra ($Z4$, $Z5$, $Z6$) having the same angular distribution as the rhombic triancontahedron itself. Similarly, we have an analysis of the rhombic triacontahedron of insert 2 into the polyhedra $N5$, $N6$, and $N7$. These polyhedra and the $Z7$ differ from the previous polyhedra $Z4$, $Z5$, $Z6$, and $N4$ only in orientation and have the same relationship as the previous polyhedra to the symmetry axes of $N2$ and $Z2$ (see above). In order for one to conceptualize the difference in orientation between the two rhombic triancontahedra (inserts 1 and 2), it is enough to observe that each of these two polyhedra or any of their component polyhedra as shown in Figure 1) results from the other (with the same name) via a rotation of 90° around any $C4$ axis of the hexahedron which is a common member polyhedron to both of them. (More details on the analysis of polyhedra into simpler ones are given in Appendix E.)

The orientation of $N9$ can easily be visualized, if one considers the centers of its triangular faces (instead of the faces themselves) which form a dodecahedron. This imaginary dodecahedron has an identical orientation to that of $N6$. Furthermore, if one wants to comprehend in more details the relationship of $N9$ to the regular polyhedra, he should consider the crossing points of an icosahedron and its reciprocal rhombic triancontahedron (as shown in Figure 4, column 6, row 3) which form a rhombicosidodecahedron as the $N9$.

APPENDIX C: RADIAL SIZES OF EQUILIBRIUM POLYHEDRA SHELLS

The radial size of each polyhedral shell (R_x) is determined solely from the knowledge of the radial size of the previous contacting polyhedral shell (R), from the minimum nucleon-nucleon separation distance of these two shells, and from a characteristic angle (α) depending on the kind of polyhedra in contact and their relative orientation.

For this purpose we employ Figure 5, which shows for each polyhedral shell a nucleon sphere labelled with the notation of this polyhedron according to Figure 1. All nucleon spheres presented in the figure are in contact and are shown in the correct radial and angular relationships to each other in agreement with the relative orientations and sizes of polyhedral shells as shown in Figure 1.

Take now, for example, the triangle $0(Z4)(N4)$ which is shown in Figure 5 and is defined by the nuclear center (0) and the centers of the nucleon spheres labeled $Z4$ and $V4$. Then, from the law of cosine we have

$$d^2 = R_x^2 + R^2 - 2R_x R \cos \alpha \qquad \text{(C.1)}$$

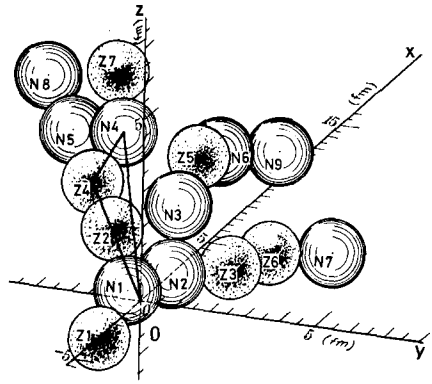

Fig. 5. Close packing of equilibrium polyhedral shells. Each polyhedral shell is represented by one of its nucleon spheres labeled with the notation of this polyhedron according to Figure 1. The representative nucleon spheres are in contact and are shown in the correct radial and angular relationships to each other in agreement with the relative orientations and sizes of polyhedral shells, as shown in Figure 1. The triangle $0(Z4)(N4)$ shown is a typical one used in the analysis for the radial determination of the momentary dynamic average forms of nuclear shells from ^{4}He to ^{208}Pb. Through this figure one can visualize the order in which the different polyhedral shells are in contact. This order corresponds to the closest packing possible of the specific polyhedral shells presented. Such close packing results in the smallest polyhedral shell radii, given that the kind of polyhedron employed in the model are already specified by assumption (a).

from which we get

$$R_x = R\cos\alpha + (d^2 - R^2\sin^2\alpha)^{1/2} \tag{C.2}$$

where

$$d = d_{NiNj} = 2r_n = 2(0.974) = 1.948 \text{ fm}$$

or

$$d = d_{ZiZj} = 2r_p = 2(0.860) = 1.720 \text{ fm} \tag{C.3}$$

or

$$d = d_{NiZj} = d_{ZiNj} = r_n + r_p = 1.834 \text{ fm}$$

For the particular example we have considered, we have from Table IV (row 10, columns 2, 3, and 4)

$$R = R_{Z4} = 4.261 \text{ fm}$$

$$d = d_{Z4,N4} = 1.834 \text{ fm}$$

and

$$\hat{\alpha} = 20^\circ\, 54'\, 19''$$

Table IV. Radial Size Determination of Equilibrium Polyhedral Shells

Polyhedra in contact according to Figure 5	R (fm)	d (fm)	α according to Figure 5	α according[a] to Table III	R_x (fm)
$N1$	0.974	0	$(N1)\,0\,(N1) = 0°$		$R_{N1} = 0(N1) = r_n = 0.974$
$N1, Z1$	0.974	1.834	$(Z1)\,0\,(N1) = 90°$		$R_{Z1} = 1.554$
$N1, N2$	0.974	1.948	$(N2)\,0\,(N1) = 45°$	ϕ_8	$R_{N2} = 2.511$
$N1, Z2$	0.974	1.834	$(Z2)\,0\,(N1) = 35° 15' 52''$	ϕ_6	$R_{Z2} = 2.541$
$N2, N3$	2.511	1.948	$(N3)\,0\,(N2) = 31° 43' 03''$	ϕ_{20}	$R_{N3} = 3.568$
$N2, Z3$	2.511	1.834	$(Z3)\,0\,(N2) = 20° 54' 19''$	ϕ_{12}	$R_{Z3} = 3.946$
$Z2, Z4$	2.541	1.720	$(Z4)\,0\,(Z2) = 0°$		$R_{Z4} = 4.261$
$N3, Z5$	3.568	1.834	$(Z5)\,0\,(N3) = 0°$		$R_{Z5} = 5.402$
$Z3, Z6$	3.946	1.720	$(Z6)\,0\,(Z3) = 0$		$R_{Z6} = 5.666$
$Z4, N4$	4.261	1.834	$(N4)\,0\,(Z4) = 20° 54' 19''$	ϕ_{12}	$R_{N4} = 5.006$
$Z4, N5$	4.261	1.834	$(N5)\,0\,(Z4) = 0°$		$R_{N5} = 6.095$
$Z5, N6$	5.402	1.834	$(N6)\,0\,(Z5) = 10° 48' 44''$	$\phi_{20} - \phi_{12}$	$R_{N6} = 6.835$
$Z6, N7$	5.666	1.834	$(N7)\,0\,(Z6) = 10° 48' 44''$	$\phi_{20} - \phi_{12}$	$R_{N7} = 7.060$
$N4, Z7$	5.006	1.834	$(Z7)\,0\,(N4) = 0°$		$R_{Z7} = 6.840$
$N5, N8$	6.095	1.948	$(N8)\,0\,(N5) = 0°$		$R_{N8} = 8.043$
$N6, N9$	6.835	1.948	$(N9)\,0\,(N6) = 10° 48' 44''$	$\phi_{20} - \phi_{12}$	$R_{N9} = 8.180$

[a] $\phi_{i(=6,8,12,20)}$ denotes the angle ϕ of the polyhedron with number of faces equal to i[$= 6$(hexahedron), 8 (octahedron), 12 (dodecahedron), and 20 (icosahedron)], according to Table III.

Hence, from equation (C.2)

$$R_x = R_{N4} = (4.261)\cos(20° 54' 19'') + [(1.834)^2 - (4.261)^2 \sin^2(20° 54' 19'')]^{1/2} = 5.006 \text{ fm} \quad \text{(C.4)}$$

(see row 10, column 6 of Table IV). In order now for one to construct Table IV, he starts from the first row, where all items are known, and proceeds row by row. Specifically, column 1 includes the notations of pairs of polyhedra in contact (according to Figure 5), the first of them having a known radial size [which is listed in a previous row of the table (column 6) and repeated in column 2 (same row)] and the second being the polyhedron whose radial size is under determination. Column 3 includes values from equation (C.3), the specific value for a particular row depending on the polyhedra of column 1 in this row, i.e., if both are neutron, or both are proton, or the one neutron and the other proton polyhedra. Columns 4 and 5 include the values of the characteristic angle α, where in the former column this angle is specified using Figure 5 and its numerical value is

given, while in the latter column the same angle using notations of characteristic regular polyhedra angles from Table III is given.

APPENDIX D: SAMPLE CALCULATIONS

In this appendix we give all sample calculations necessary for a complete understanding of the numerical predictions of the classical part of the isomorphic model for closed-shell nuclei as listed in Table I. We take ^{40}Ca as an example, where three shells for protons ($Z1$, $Z2$, and $Z3$) and three shells for neutrons ($N1$, $N2$, and $N3$) are involved, with numbers of nucleons 2, 6, and 12, respectively, both for protons (Z) and for neutrons (N) and with radii (fm) 1.554, 2.541, 3.946, 0.974, 2.511, and 3.568, respectively (see the first three levels of Figure 1, viz., Figures 1A–1C, 1a–c. Charge root mean square radius [equation (2)]:

$$\langle r^2\rangle_{ch}^{1/2\ ^{40}\mathrm{Ca}} = \left[\frac{2(1.554)^2+6(2.541)^2+12(3.946)^2+20(0.8)^2-20(0.34)^2}{20}\right]$$
$$= 3.47 \text{ fm} \tag{D.1}$$

Neutron–proton root mean square radial difference [equation (3)]:

$$\langle r^2\rangle_n^{1/2} - \langle r^2\rangle_p^{1/2} \equiv \Delta r_{np}\ ^{40}\mathrm{Ca}$$
$$= \left[\frac{2(0.974)^2+6(2.511)^2+12(3.568)^2}{20}\right]^{1/2}$$
$$-\left[\frac{2(1.554)^2+6(2.541)^2+12(3.946)^2}{20}\right]^{1/2}$$
$$= -0.29 \text{ fm} \tag{D.2}$$

Average nuclear density [equation (4)]:

$$\langle r^2\rangle_{\text{mass}}^{1/2} = \left[\frac{2(1.554)^2+6(2.541)^2+12(3.946)^2+2(0.974)^2}{40}\right.$$
$$\left.+\frac{6(2.511)^2+12(3.568)^2+20(0.860)^2+20(0.974)^2}{40}\right]^{1/2}$$
$$= 3.38 \text{ fm} \tag{D.3}$$
$$R_{\text{eq}} = (5/3)^{1/2}\langle r^2\rangle_{\text{mass}}^{1/2} = (5/3)^{1/2}(3.38) = 4.36 \text{ fm}$$
$$d = \frac{40}{(4/3)\pi R_{\text{eq}}^3} = \frac{40}{(4/3)\pi(4.36)^3} = 0.115 \frac{\text{nucleons}}{(\text{fm})^3}$$

Radial parameter r_0 [equation (5)]:

$$r_0 = \{(4\pi/3)d\}^{-1/3} = \{(4\pi/3)(0.115)\}^{-1/3} = 1.28 \frac{\text{fm}}{(\text{nucleon})^{1/3}} \qquad \text{(D.4)}$$

APPENDIX E: CREATION OF HOLES AND "ANALYSIS" OF EQUILIBRIUM POLYHEDRA INTO SIMPLER ONES

As one can see from Figure 1 some polyhedra vertices are unoccupied (are empty, called holes), and some equilibrium polyhedra are analyzed into simpler equilibrium polyhedra (called member polyhedra of the initial polyhedron). The explanation of both is the purpose of the present appendix.

Creation of holes: We use again ^{40}Ca as an example. If we consider now that the $Z3$ in Figure 1 (that is, the last proton polyhedron in ^{40}Ca) has no empty vertices but protons are assumed at its vertices labeled h, then these proton spheres overlap with the proton sphere of the $Z1$, since $R_{Z2} - R_{Z1} = 2.541 - 1.554 = 0.987$ fm. Indeed, this difference of the radii of the exscribed spheres of the polyhedra $Z1$ and $Z2$ defined by the proton centers is smaller than the double of the proton radius $r_p = 0.860$ fm (minimum distance of proton sphere centers when they are in contact). Since such an overlapping is against assumption (b), where hard spheres are assumed, we have the creation of holes in the $Z2$. These holes form a cube (hexahedron). The $Z4$ is really the smallest cube that can be filled after $Z2$ and is in contact with it. One could think that we can avoid the holes in the $Z3$ by increasing its radius to become equal to the radius of the $Z4$. In this case only proton spheres of the $Z3$ at the vertices labeled h would be in contact with proton spheres of the $Z2$. All other proton spheres of $Z3$ would not be in contact with any sphere. In such a situation one could easily show that the rms charge radius of ^{40}Ca (and of the next closed-shell nuclei) would be much larger than the experimental value, while the binding energy would be much smaller.

The existence of holes at an equilibrium polyhedron does not violate the condition of equilibrium of particles assumed at the remaining vertices, when these holes are distributed in such a way on the polyhedron that they form another equilibrium polyhedron. Such are the cases of holes in all parts of Figure 1.

Analysis of Polyhedra: As an example, we take now the rhombic triancontahedron of insert 1, which is analyzed into three member polyhedra, namely, the $Z4$, $Z5$, and $Z6$. If such an analysis did not happen, the $Z4$ would have to increase its size to take the place of the holes in the $Z6$, and the $Z5$ would also have to increase its size so that its edges and the edges of the $Z6$ could bisect each other at right angles (see Figure 4, column 5,

row 3 and caption of this figure) in order for the vertices of $Z5$ and $Z6$ to form the rhombic triancontahedron. Then, the $Z5$ and $Z6$ would have a common middle sphere ($_1R$) for which from Table III we would have

$$_1R_{12} = 2.6180 L_{12} = 2.6180\left(\frac{_0R_{12}}{2.8026}\right) \tag{E.1}$$

$$_1R_{20} = 1.6180 L_{20} = 1.6180\left(\frac{_0R_{20}}{1.9020}\right) \tag{E.2}$$

and since $_1R_{12} = {}_1R_{20}$ we would get

$$_0R_{20} = (1.098)\ {}_0R_{12} \tag{E.3}$$

or

$$R_{Z5} = (1.098) R_{Z6} = 6.222 \text{ fm} \tag{E.4}$$

Obviously, these new sizes of the $Z4$ and $Z5$ would lead to much larger rms charge radii and much smaller binding energies for all closed-shell nuclei having these polyhedra in their isomorphic structure. Thus, this analysis serves the same purpose as the existence of holes. The analysis of an equilibrium polyhedron into member polyhedra does not violate the condition of equilibrium of particles assumed at the vertices of the initial polyhedron, as long as each of the member polyhedra is an equilibrium polyhedron. Obviously, the anglar vertex distribution of the initial polyhedron is identical with the angular vertex distributions of the derived polyhedra taken together. All the analyses of polyhedra made in Figure 1 are of such a type.

REFERENCES

Alkhazov, G. D., Belostotsky, S. L., Domchenkov, O. A., Dotsenko, Yu. V., Kuropatkin, N. P., Nickulin, V. N., Shuvaev, M. A., and Vorobyov, A. A. (1976). In Proc. Int. Conf. on the Radial Shape of Nuclei, M. Guenin, ed., pp. 47–48.

Anagnostatos, G. S. (1973). *Canadian Journal of Physics*, **51**, 998.

Anagnostatos, G. S. (1977). *Atomkernenergie*, **29**, 207.

Anagnostatos, G. S. (1978). *Lettere al Nuovo Cimento*, **22**, 507.

Anagnostatos, G. S. (1980a). *Lettere al Nuovo Cimento*, **28**, 573.

Anagnostatos, G. S. (1980b). *Lettere al Nuovo Cimento*, **29**, 188.

Anagnostatos, G. S., and Panos, C. N. (1982). *Physical Review C*, **26**, 260.

Anagnostatos, G. S., Touliatos, S., Kyritsis, A., and Yapitzakis, J. (1980). *Atomkernenergie*, **35**, 60.

Anagnostatos, G. S., Yapitzakis, J, and Kyritsis, A. (1981). *Lettere al Nuovo Cimento*, **32**, 332.

Bernstein, A. M., and Seidler, W. A. (1972). *Physics Letters* **39B**, 583.

Bertozzi, W., Friar, J., Heisenberg, J., and Negele, J. W. (1972). *Physics Letters*, **41B**, 408.

Bertsch, G. F. (1983). *Scientific American*, **248**, 40.
Brown, B. A., Massen, S. E., and Hodgson, P. E. (1979). *Journal of Physics G*, **5**, 1655.
Celenza, L. S., and Shakin, C. M. (1983). *Physial Review C*, **27**, 1561.
Cook, N. D. (1976). *Atomkernenergie.* (1978). **28**, 195.
Coxeter, H. S. M. (1963). *Regular Polytopes*, 2nd edition, Macmillan, New York.
de Boer, J., and Mang, H. J., eds. (1973). Proceedings of the International Conference on Nuclear Physics, p. 101.
de Jager, C. W., de Vries, H., and de Vries, C. (1974). *Atomic Data and Nuclear Data Tables*, **14**, 479–508.
Engfer, R., Schneuwly, H., Vuilleumier, J. L., Walter, H. K., and Zehnder, A., *Atomic Data and and Nuclear Data Tables*, **14**, 509–597.
Greenless, G. W., Hnizdo, V., Karban, O., Lowe, J., and Makofske, W. (1970). *Physical Review C* **2**, 1063.
Hill, D. L. (1957). In *Encyclopedia of Physics*, S. Flugge, ed., Springer-Verlag, Berlin, Vol. XXXIX, p. 211.
Hodgson, P. E. (1980). Invited paper presented at the Workshop in Nuclear Physics, Drexell University.
Hodgson, P. E. (1981). Invited paper presented at the IV International Symposium on Nuclear Physics, Oaxtepec, Mexico.
Holden, N. E, and Walker, F. W. (1972). *Chart of the Nuclides*, 11th edition, General Electric Co., Schenectady, New York.
Hornyak, W. F. (1975). *Nuclear Structure*, Academic, New York, p. 194.
Inglis, D. R. (1969). *Physics Today*, **22**, 29.
Jackson, D. F. (1976). Invited paper presented at the Int. Conf. on the Radial Shape of Nuclei, A. Budzanowski and A. Kapuscik, eds., pp. 141–161.
Kaplan I. (1962). *Nuclear Physics*, 2nd edition, Addison-Wesley, Reading Massachusetts, p. 222.
Leech, J. (1957). *Mathematical Gazette*, **41**, 81.
Margenau, H. (1941). *Physical Review*, **59**, 37.
Mariscotti, M. A. J., Scharff-Goldhaber, G., and Buck, B. *Physical Review*, **178**, 1864.
Mayer, M. G., and Jensen, J. H. D. (1955). *Elementary Theory of Nuclear Shell Structure*, Wiley, New York, p. 58.
Moszkowski, S. A. (1957). In "Models of nuclear structure," in *Encyclopedia of Physics*, S. Flügge, Springer-Verlag, Berlin, Vol. 39, pp. 411–450.
Negele, J. W. (1976). Invited paper presented at the Int. Conf. on the Radial Shape of Nuclei, A. Budzanowski and A. Kapuscik, eds., pp. 79–102.
Nolen, J. A., and Schiffer, J. P. (1969). *Annual Review of Nuclear Science*, **19**, 471.
Panos, C. N., and Anagnostatos, G. S. (1982a). In Proc. Int. Conf. on Nuclear Structure, A. van der Woude and B. J. Verhaar, eds., p. 58.
Panos, C. N, and Anagnostatos, G. S. (1982b). *Journal of Physics G*, **8**, 1651.
Paulin, L. (1965a). *Science*, **150**, 297.
Pauling, L. (1965b). *Nature*, **206**, 174.
Pyle, G. J., and Greenless, G. W. (1969). *Physical Review*, **181**, 1444.
Rebel, H. (1976). Invited paper presented at the Int. Conf. on the Radial Shape of Nuclei, A. Budzanowski and A. Kapuscik, eds., pp. 163–210.
Robson, D. (1978). *Nuclear Physics*, **A308**, 381.
Stock, H. (1976). Invited paper presented at the Int. Conf. on the Radial Shape of Nuclei, A. Budzanowski and A. Kapuscik, eds., pp. 103–139.
Svenne, J. P. (1980). *Journal of Physics G*, **6**, 465.
Théberge, S., and Thomas, A. W. *Nuclear Pjysics A*, **393**, 252.

Thomas, A. W. (1983). ref. TH. 3552-CERN, March.
Trainor, L. E. H., and Gupta, R. K. (1971). *Canadian Journal of Physics*, **49**, 133.
Wapstra, A. H., and Gove, N. B. (1971). *Nuclear Data Tables*, **9**, 267.
Wilkinson, D. H. (1977). *Nuclear Instruments and Methods*, **146**, 143.